



HAL
open science

POLAR project: a numerical study to optimize the target design

C Busschaert, É Falize, B Loupias, C Michaut, A Ravasio, A Pelka, R Yurchak, M Koenig

► To cite this version:

C Busschaert, É Falize, B Loupias, C Michaut, A Ravasio, et al.. POLAR project: a numerical study to optimize the target design. *New Journal of Physics*, 2013, 15, pp.035020. 10.1088/1367-2630/15/3/035020 . hal-01586948

HAL Id: hal-01586948

<https://hal.sorbonne-universite.fr/hal-01586948v1>

Submitted on 13 Sep 2017

HAL is a multi-disciplinary open access archive for the deposit and dissemination of scientific research documents, whether they are published or not. The documents may come from teaching and research institutions in France or abroad, or from public or private research centers.

L'archive ouverte pluridisciplinaire **HAL**, est destinée au dépôt et à la diffusion de documents scientifiques de niveau recherche, publiés ou non, émanant des établissements d'enseignement et de recherche français ou étrangers, des laboratoires publics ou privés.



Distributed under a Creative Commons Attribution 4.0 International License

PAPER • OPEN ACCESS

POLAR project: a numerical study to optimize the target design

To cite this article: C Busschaert *et al* 2013 *New J. Phys.* **15** 035020

View the [article online](#) for updates and enhancements.

Related content

- [SIMILARITY PROPERTIES AND SCALING LAWS OF RADIATION HYDRODYNAMIC FLOWS IN LABORATORY ASTROPHYSICS](#)
É. Falize, C. Michaut and S. Bouquet
- [Propagation of laser-generated plasma jet in an ambient medium](#)
B Loupias, E Falize, C D Gregory *et al.*
- [Accretion Flow in Magnetic Cataclysmic Variables](#)
Kinwah Wu, Mark Cropper, Gavin Ramsay *et al.*

Recent citations

- [Laboratory analogue of a supersonic accretion column in a binary star system](#)
J. E. Cross *et al*
- [Target fabrication for the POLAR experiment on the Orion laser facility](#)
C. Spindloe *et al*
- [Formation and propagation of laser-driven plasma jets in an ambient medium studied with X-ray radiography and optical diagnostics](#)
A. Dizière *et al*

POLAR project: a numerical study to optimize the target design

**C Busschaert^{1,2,4}, É Falize^{1,2}, B Loupias², C Michaut¹,
A Ravasio³, A Pelka³, R Yurchak³ and M Koenig³**

¹ LUTH Observatoire de Paris, CNRS, Université Paris Diderot,
F-92190 Meudon, France

² CEA-DAM-DIF, F-91297 Arpajon, France

³ LULI, CNRS-CEA, Université Paris VI, Ecole Polytechnique,
F-91128 Palaiseau, France

E-mail: clotilde.busschaert@obspm.fr

New Journal of Physics **15** (2013) 035020 (14pp)

Received 20 September 2012

Published 20 March 2013

Online at <http://www.njp.org/>

doi:10.1088/1367-2630/15/3/035020

Abstract. Modern high-energy density facilities allow us to bring matter to extreme states of density, temperature and velocity. Rigorous scaling laws proved that the relevant regimes could be reached, and those regimes are reproducibly achievable. Using powerful lasers and adapted target designs, similarity experiments in the POLAR project aim at studying the formation and dynamics of accretion shocks as found in magnetic cataclysmic variables. At the astrophysical scale, the system we consider is a column of infalling plasma collimated by a magnetic field onto the surface of a white dwarf. As matter hits the surface with supersonic velocity, a shock forms at the basis of the column and propagates upstream. In this paper, numerical simulations are presented in order to describe the experience and to give expectations concerning physical regimes reachable for future experiments on a kilojoule facility. In particular, our target design is discussed and improvements are detailed.

⁴ Author to whom any correspondence should be addressed.



Content from this work may be used under the terms of the [Creative Commons Attribution-NonCommercial-ShareAlike 3.0 licence](https://creativecommons.org/licenses/by-nc-sa/3.0/). Any further distribution of this work must maintain attribution to the author(s) and the title of the work, journal citation and DOI.

Contents

1. Introduction	2
2. Similarity properties and scaling laws	3
3. Experimental simulations of accretion processes in polar experiments	5
4. Astrophysical relevance of laboratory experiments	11
5. Conclusion	13
Acknowledgments	13
References	13

1. Introduction

Magnetic cataclysmic variables are semi-detached binary systems containing a highly magnetized white dwarf accreting material coming from its Roche-lobe-filling companion (see, e.g., Warner 1995 and Wu 2000 for reviews). In particular, we are interested in systems named AM Her stars or polars where the white dwarf has a magnetic field higher than 10 MG. In those objects, the magnetic field is strong enough to prevent the formation of an accretion disc around the white dwarf. Material leaving the companion is tied to the field lines of the white dwarf magnetic field and then led toward the magnetic poles of the compact star where accretion columns form. When the supersonic flow ($u_{ff} \sim 5000 \text{ km s}^{-1}$) falls onto the white dwarf surface, a radiative shock wave is produced and propagates through the column upstream. In the post-shock region, matter reaches extreme physical conditions ($T \sim 10^8 \text{ K}$, $\rho \sim 10^{-7} - 10^{-4} \text{ g cm}^{-3}$) and produces most of the high-energy radiation emitted by the system. Radiative processes induce a cooling behind the shock front, which structures the profile of density, temperature and velocity since the typical dynamical time is longer than the cooling time scale (Chevalier and Imamura 1982). Considering the current theoretical scheme, some observational issues remain controversial. For example, quasi-periodic oscillations in the light curve are observed in optical wavelengths (Larsson 1992) but not in x-rays, or the energy balance between soft and hard x-ray emissions in some polars (Ramsay and Cropper 2004), which cannot be explained by considering the numerical forecasting at the astrophysical scale with the current model. Moreover, the determination of the white dwarf mass based on the radiation emitted at the basis of the column is still highly model dependent (Cropper *et al* 1998).

Modern high-energy facilities give us an opportunity to have a new point of view of those objects, since reaching extreme conditions of density and temperature has now become achievable (Remington *et al* 2006, Savin *et al* 2012). Our objective is to get a better understanding of the post-shock structure. Using scaling laws, it can be possible to generate flows similar to astrophysical ones in the laboratory (Ryutov *et al* 1999, Falize *et al* 2009). Moreover, we can take advantage of diagnostics which allow good characterization of the plasma during the experiment. This is not feasible today at the astrophysical scale, given that the accretion column is approximately 1000 km long and thus unresolved. Furthermore, in the laboratory, we can try to control boundary conditions and parameters of the system which are important for testing predominant physical mechanisms linked with radiation processes that occur in this high-energy environment. The experience has recently been validated and tested (Falize *et al* 2012).

In this context, we present new target designs which can allow one to get closer to similar regimes to those encountered at the astrophysical scale. In the first place, we present scaling laws defining the relevant experimental regime and similarity properties of our system. Then, based on numerical simulations, we analyze the target behavior. In particular, the new proposed target designs include a mass reservoir. This mass reservoir allows us to get a more homogeneous flow for a longer time, which is precisely the crucial point of the experiment. Using a light foam to fill the mass reservoir, we also manage to reach higher flow velocity and thus higher post-shock temperature after the impact. To conclude, the astrophysical relevance of laboratory flows is discussed and similarity properties predicted by numerical simulation are presented.

2. Similarity properties and scaling laws

According to the physical regime of the post-shock region, several hypotheses can be made to describe the accretion column (Lamb and Masters 1979, Busschaert *et al* 2013). The medium can be considered as optically thin for bremsstrahlung emission since the mean free path is larger than the typical radius of the column for x-ray wavelength radiation. The shock is collisional considering that the typical time scale associated with ion–ion collision is shorter than the dynamical timescale (Langer *et al* 1982). We can also assume that for a low-mass white dwarf ($M < 1 M_{\odot}$), the post-shock region can be correctly modeled by a single temperature medium (Wu *et al* 1994) and the external field of gravitation generated by the white dwarf can be locally neglected since the column height is quite small compared to the white dwarf radius. Finally, the curvature of the white dwarf surface can be neglected since the column seems to cover only a small fraction of the white dwarf surface (see, e.g., Ramsay and Cropper (2007) for an observational estimation).

For a given white dwarf mass—on which depends the infalling free-fall velocity—accretion rate and magnetic field are the two main parameters driving the system geometry and radiative emission in magnetic cataclysmic variables (see figure 1). For $B < 10$ MG, magnetic cataclysmic variables are called intermediate polars. Depending on the spin period of the white dwarf and the orbital period of the binary system, four accreting geometries can take place in those astrophysical systems: discs, streams, rings and propellers (Norton *et al* 2008). In this paper, we are interested in the specific case of polars with $B > 10$ MG. When the accretion rate is relatively high, $\dot{m} \sim 1\text{--}100 \text{ g cm}^{-2} \text{ s}^{-1}$, and $B \sim 10\text{--}30$ MG, bremsstrahlung emission dominates the cooling processes in the column (figure 1, black zone (1)). In this regime, the only significant effect of the magnetic field is to channel the flow of plasma toward the magnetic poles. For higher magnetic field and lower accretion rate, cyclotron emission can no longer be negligible as a cooling process (figure 1, gray zone (2)). As the accretion rate decreases below $\dot{m} \sim 1 \text{ g cm}^{-2} \text{ s}^{-1}$ for $B \sim 10$ MG, not only the cyclotron has to be considered but also the two-temperature effects (figure 1, white zone (3)). For still lower accretion rate or higher magnetic field, the flow can no longer be considered as collisional. No reverse shock can be formed in the flow and the accretion regime is modeled by a bombardment solution that seems to well describe the specific class of low accretion rate polars (Schmidt *et al* 2005).

For each polar regime, a scaling law can be defined (regimes (1) and (2) demonstrated in Falize *et al* (2011a) and regime (3) in Falize *et al* (2011b)). For now, we focus on the regime where cooling is dominated by the bremsstrahlung process (regime (1), figure 1), since then the magnetic field only collimates the flow. Thus, an adapted description of the plasma is obtained

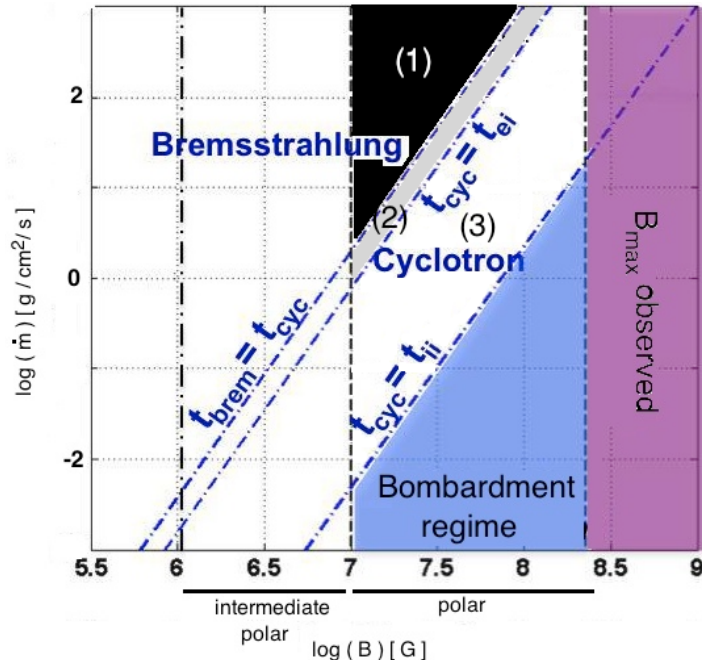


Figure 1. Diagram of the specific accretion rate versus magnetic field showing the different regimes of accretion in the case of magnetic cataclysmic variables for a white dwarf of 1 solar mass. Intermediate polars have $B < 10$ MG; polars have $B > 10$ MG. For polars, when the accretion rate is high ($\dot{m} \sim 1\text{--}100 \text{ g cm}^{-2} \text{ s}^{-1}$) and $B \sim 10\text{--}100$ MG (black zone (1)), bremsstrahlung dominates the radiative cooling. This black-colored zone corresponds to the regime we focus on in laboratory experiments. For higher B and lower accretion rate (gray zone (2)), cyclotron emission cooling cannot be neglected, and for still lower accretion rate or higher magnetic field (white zone (3)), cyclotron dominates the cooling and two-temperature effects have to be taken into account. Based on Lamb and Masters (1979) and Wickramasinghe *et al* (2000).

by the following system of equations:

$$\begin{cases} \partial_t \rho + \nabla \cdot (\rho \mathbf{u}) = 0, \\ \partial_t (\rho \mathbf{u}) + \nabla \cdot (\rho (\mathbf{u} \otimes \mathbf{u}) + p \mathbf{I}) = 0, \\ \partial_t E + \nabla \cdot ((E + p) \mathbf{u}) = -\Lambda(\rho, p), \end{cases} \quad (1)$$

where ρ is the density, \mathbf{u} the velocity, p the thermal pressure and E the total energy density. The total energy is the sum of the kinetic and internal energies, $E = \rho u^2/2 + \rho e$. The function $\Lambda(\rho, p)$ models energy losses by radiative processes. These are defined as a power law of density and pressure $\Lambda = \Lambda_0 \rho^\epsilon p^\zeta$, where Λ_0 , ϵ , ζ are three constants characterizing the mechanism causing the cooling in specific domains of density and temperature. Bremsstrahlung cooling is modeled by the cooling function $\Lambda = \Lambda_0 \rho^{3/2} p^{1/2}$, with $\Lambda_0 = 3.9 \times 10^{11} \text{ J m}^{-2} \text{ s}^{-1}$ (Rybicki *et al* 1986). Such an expression allows one to develop a model that accepts analytical solutions (Chevalier and Imamura 1982, Falize *et al* 2009).

To establish scaling laws between the astrophysical and the laboratory system, both have to be driven by the same physics and then described by the same equations. Moreover, each system needs to satisfy boundary and initial conditions verifying the scaling laws. The one-parameter homothetic Lie group (Bluman and Cole 1974) is used to relate quantities at the astrophysical (X_a) and laboratory (X_l) scale. It is defined by $X_a = \lambda^{\delta_X} X_l$, where λ and δ_X are, respectively, the group parameter and the homothetic exponent specific to each quantity. The absolute similarity is the classical approach, which consists in the rescaling of independent (x, t) and dependent (ρ, p, T, u) variables. The more general global similarity framework does not require conservation of the sub-physical scales, which adds additional free parameters (Falize *et al* 2011a).

In the framework of absolute similarity, exact scaling laws between quantities at the astrophysical and laboratory scale, with the subscripts a and l, respectively, can be constructed:

$$\begin{aligned} \frac{\rho_a}{\rho_l} &= \lambda^\alpha, & \frac{p_a}{p_l} &= \lambda^\beta, & \frac{T_a}{T_l} &= \lambda^{\beta-\alpha}, \\ \frac{u_a}{u_l} &= \lambda^{(\beta-\alpha)/2}, & \frac{t_a}{t_l} &= \lambda^{(\beta-3\alpha)/2}, & \frac{x_a}{x_l} &= \lambda^{\beta-2\alpha}, \\ \frac{\epsilon_{0,a}}{\epsilon_{0,l}} &= 1, & \frac{\Lambda_{0,a}}{\Lambda_{0,l}} &= 1 \end{aligned} \quad (2)$$

with L and t , respectively, the length and time in our system and α, β , two constant free scaling parameters. We assume that pressure, density and temperature are linked by the relation $P = \epsilon_0 \rho T$. In the global similarity framework, the scaling laws become

$$\begin{aligned} \frac{\rho_a}{\rho_l} &= \lambda^\alpha, & \frac{p_a}{p_l} &= \lambda^\beta, & \frac{T_a}{T_l} &= \lambda^{(\beta-\psi-\alpha)}, \\ \frac{u_a}{u_l} &= \lambda^{(\beta-\alpha)/2}, & \frac{t_a}{t_l} &= \lambda^{(\beta-3\alpha+\psi)/2-\delta}, & \frac{x_a}{x_l} &= \lambda^{\beta-2\alpha-\delta+\psi/2}, \\ \frac{\epsilon_{0,a}}{\epsilon_{0,l}} &= \lambda^\psi, & \frac{\Lambda_{0,a}}{\Lambda_{0,l}} &= \lambda^\delta, \end{aligned} \quad (3)$$

where ψ and δ are two additional scaling parameters.

The scaling laws expressed above (equations (2) and (3)) give the typical scales needed for the laboratory experiments, see table 1. Consequently, astrophysical systems can be modeled in the laboratory with a system whose typical length is of the order of a few millimeters and which evolves on a timescale of the order of a few tens of nanoseconds. The experiment has to be so designed as to get a flow of plasma which reaches a post-shock temperature of the order of 100 eV with an infalling density of the order of 10 mg cm^{-3} and a flow velocity around 300 km s^{-1} . Such a regime of velocity, temperature and density can be reached using a megajoule laser facility.

3. Experimental simulations of accretion processes in polar experiments

To reproduce the astrophysical phenomenon in the laboratory, an experimental design has been established. As a first step, we validate the experimental concept of our target on a kilojoule facility. The following numerical simulations are done in the conditions of the LULI2000 facility with a high-energy long pulse laser beam characterized by $E \sim 300 \text{ J}$ at 2ω ($\lambda_L = 527 \text{ nm}$) with

Table 1. Typical scale of the two systems of interest: the astrophysical and laboratory accretion columns when applying the scaling laws of absolute invariance expressed above (equation (2)). The key parameters are: the column height, x , the dynamical timescale, t , the inflow velocity, u , the infalling plasma density, ρ , and the post-shocked temperature, T .

	x (m)	t (s)	u (km s ⁻¹)	ρ (g cm ⁻³)	T (K)
Polar	10 ⁵	1	3 × 10 ³	10 ⁻⁸	10 ⁸
Laboratory	10 ⁻³	10 ⁻⁷	3 × 10 ²	10 ⁻²	10 ⁶

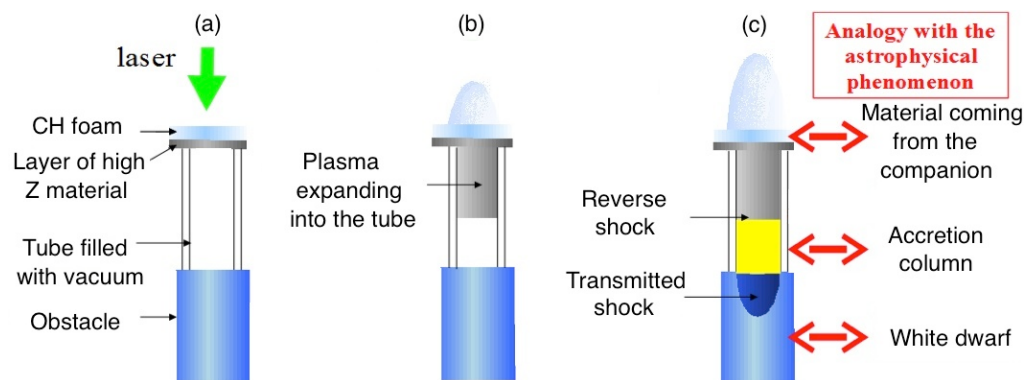


Figure 2. Experimental principle. A flow is generated by laser–matter interaction (a) and propagates into a tube (b). The supersonic flow hits an obstacle mimicking the white dwarf surface and a reverse shock is produced (c).

a typical pulse length of 1.5 ns. The focal spot diameter is typically 400 μm with a resulting intensity of $I_L \sim 10^{14} \text{ W cm}^{-2}$ (Loupas *et al* 2007).

The concept is based on the generation of a flow of plasma mimicking the material falling onto the white dwarf (see figure 2). This flow has to be supersonic in order to generate a reverse shock at the collision. An obstacle is needed which plays the role of the white dwarf surface. In order to collimate the flow, we use a tube which plays the role of the magnetic field confinement. We have studied two types of flows: the first one from a solid driver used during the first POLAR experiment (Falize *et al* 2012) and the second one from a foam driver inspired by supersonic jet experiments (Loupas *et al* 2007) and proposed in Falize *et al* (2011c).

We will first describe the behavior of the first target design. To generate the supersonic flow, we exploit the interaction between a nanosecond laser and matter. We present one-dimensional (1D) and two-dimensional (2D) numerical simulations (see figure 3) done using the CEA laser radiation hydrodynamic ALE code FCI2 (Schurtz *et al* 2000). We use the multi-group diffusion model (100 groups) which allows one to reproduce the LULI2000 regime and the laser–matter interaction is modeled by a ray tracing algorithm. The typical resolution of the simulations is around 0.5 μm . The laser ablates the plastic layer and it launches a shock by the rocket effect. This shock propagates through the layer of plastic and then passes through the high-Z material, see figure 4(1)). We use a bi-layer pusher formed by a 10–20 μm layer of plastic (CH) and a 3–5 μm layer of high-Z material such as aluminum, titanium or tin. The high-Z layer is used to protect the obstacle from x-ray radiation produced by the hot coronal plasma. Once the shock

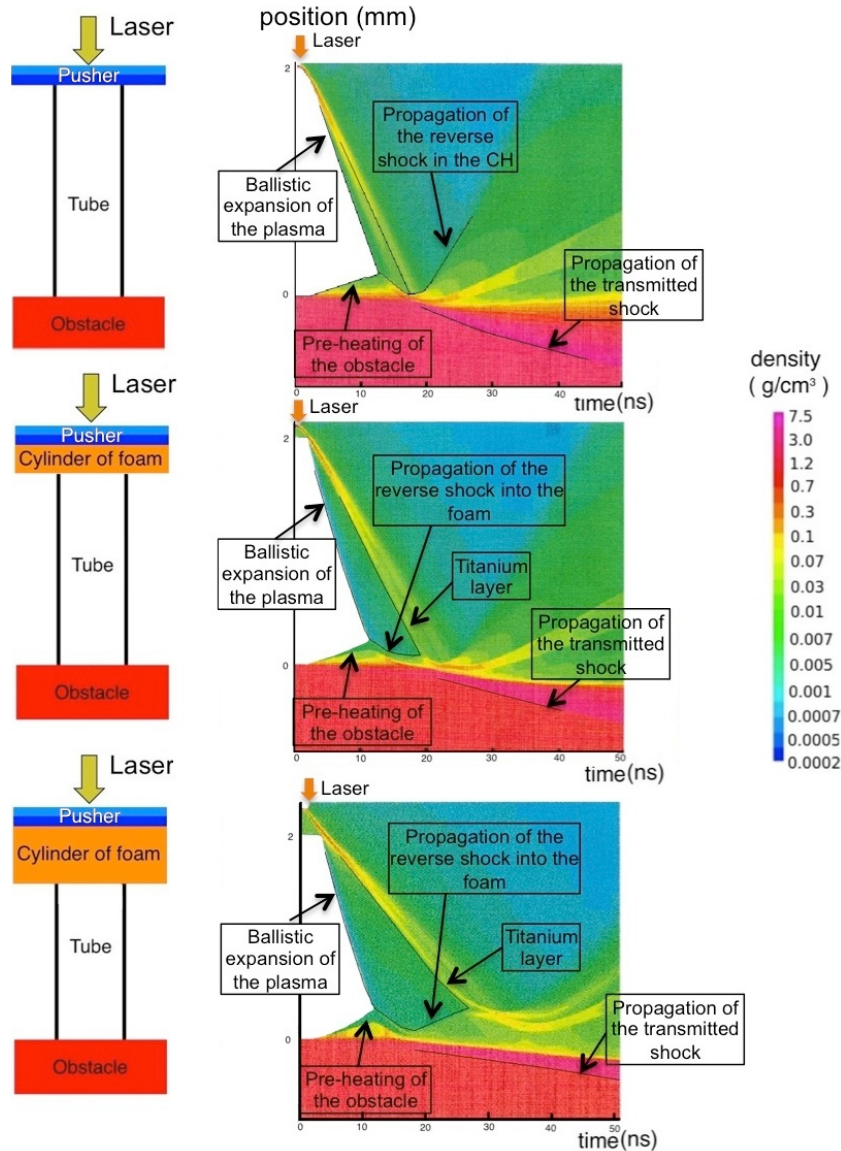


Figure 3. Top: evolution of the density (g cm^{-3}) in a typical bi-layer target, which corresponds to the first design, along the transverse direction of the target with time. The bi-layer is composed of CH ($20 \mu\text{m}$ thick) and titanium ($3 \mu\text{m}$ thick). The obstacle is a block of quartz; the pre-heating is overestimated due to the 1D approximation. Middle: the same diagram for a target with a two-layer target and a cylinder of foam corresponding to the second target design which can be approximated by a 1D system. The cylinder length is $85 \mu\text{m}$ and the foam density is 50 mg cm^{-3} . Bottom: the same diagram with the same target as the middle one except for a $250 \mu\text{m}$ long cylinder of foam.

reaches the bottom of the high- Z layer after ~ 1 ns, the shocked material is heated and ionized and the plasma begins to expand into the tube which is a few millimeters long. As can be seen in figure 3 (top), the plasma expands until reaching the obstacle. The asymptotic velocity of the flow can be estimated in the LULI conditions by the expression of a ballistic expansion

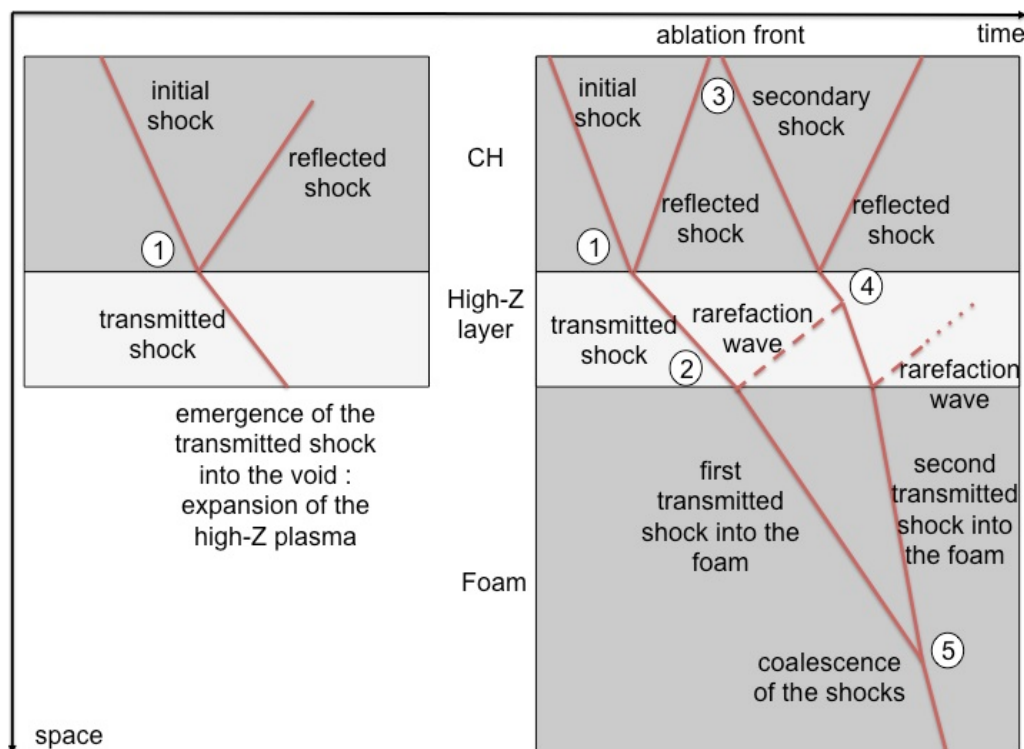


Figure 4. Dynamics of the shock propagation into the pusher of both kinds of target, without mass reservoir on the left and with a layer of foam on the right. With the first target design, when the initial shock passes through the interface between the CH and the high-Z material (1), a transmitted shock is generated along with a reflected one. When a layer of foam is added, the reflected shock generated by the initial shock passage at the interface between CH and the high-Z material (1) interacts with the thermal front generated by the ablation of the CH by the laser (3). This leads to the formation of a secondary shock which passes through the high-Z layer (4) and can lead ultimately to the coalescence of the two generated shocks propagating into the foam (5) provided that the foam thickness is large enough. If the coalescence takes place, the resulting shock is accelerated and the asymptotic velocity of the expanding plasma of foam is larger than otherwise.

(Zel'dovich and Raizer 1967), $U_{\max} \sim 150 \text{ km s}^{-1}$. A parametric study was done to optimize the composition and thickness of the two layers of the pusher and also the length of the tube. The latest is defined to get a compromise between the velocity of the expanding flow and its density. Indeed, the tube has to be long enough for the plasma to reach the maximum asymptotic velocity, but the mean density of the flow is inversely proportional to the length of the tube and must stay high enough to be diagnosed during experiments. Considering the LULI2000 properties, the best compromise is a tube of $l = 2 \text{ mm}$ for bi-layer pushers. Thus the collision time t_{coll} can be estimated by $t_{\text{coll}} \sim l/U_{\max} \sim 15 \text{ ns}$.

As the supersonic flow hits the obstacle, a reverse shock is produced inside the flow. This reverse shock propagates through the medium inside the tube, while a transmitted shock propagates through the obstacle. Numerical simulations forecast a supersonic flow with an

internal Mach number around 15 and a reverse shock characterized by a Mach number of 2 which propagates for a few nanoseconds through an inhomogeneous medium. Those numerical results are in agreement with the first experimental results (Falize *et al* 2012). Since we are interested in the evolution of the reverse shock through the incoming medium, we would like to get a homogeneous medium for the longest achievable period as in the astrophysical case. With the bi-layer target configuration, once formed, the reverse shock rapidly passes through the high- Z layer of plasma to get into the plastic plasma expanding into the tube which presents a steep density gradient (see figure 3). This multi-materials interaction and the inhomogeneity of the incoming flow make the shock dynamics more complex and also make the astrophysical relevance less obvious. Finally, the velocities we reach using such a design are not high enough. We look for a radiative medium, so the higher the temperature the better, and to get those higher temperatures we need the highest achievable velocity, $T \propto u_{\text{flow}}^2$. That is why we test a second target design where the flow of plasma is generated using a mass reservoir located just behind the bi-layer pusher. Two reservoir geometries are investigated: a cylinder of foam and a cone of foam with an opening angle Φ , the former being a generalization of the cylinder where $\Phi = 0$. The cone geometry was already used during previous experiments to generate the fastest and highest Mach number flow achievable under the LULI2000 conditions (Loupas *et al* 2007). Jets characterized by a velocity of 144 km s^{-1} and an internal Mach number of 10 were produced. Two lengths for the cylinder reservoir are under consideration: the first one, $l_1 = 85 \mu\text{m}$, to get a cylinder with a volume equal to that of the cone and thus the same contained mass, and the second one, $l_2 = 250 \mu\text{m}$, which is equal to the length of the cone. To investigate the target behavior, we considered a foam composed of CH with the same density of 50 mg cm^{-3} as that used in previous jet experiments. The geometry of the cylindrical target allows us to make a 1D approximation to describe the system in the first place (see the scheme of the target in figure 3, middle and bottom).

The general mechanisms in the target are identical. The initial shock is going through plastic, then a high- Z material layer and eventually the foam. A plasma of foam is then expanding through the tube toward the obstacle with an internal Mach number of the order of 10–20 (see figure 3, middle and bottom). The reverse shock appears in the foam and propagates upstream. For the first length, l_1 , the high- Z layer follows closely the head of the flow. So the reverse shock once formed in the foam passes rapidly through the titanium layer after a few nanoseconds. For the second length, l_2 , the reverse shock propagates for $\sim 10 \text{ ns}$ into the foam with a constant velocity $u_{\text{rev.shock}} \sim 20 \text{ km s}^{-1}$. Typical Mach number of the reverse shock considering both lengths is of the order of 2–4. This design offers a more homogeneous incoming flow compared to the first target design (see figure 3), which facilitates the comparison with the astrophysical situation. Indeed, we want to investigate the evolution of the column structure once cooling mechanisms have become strong enough to influence it. Our accreting shock then needs to be fed by a homogeneous flow for the longest achievable period in order to allow enough time for the cooling mechanism to impact the column structure. The longest cylinder of foam seems more fitted to our experimental expectations since the reverse shocks propagate for a longer time into the foam before passing through the high- Z layer. Moreover, looking at the maximum velocities reached in both flows expanding in the tube, we note that the velocities are of the order of $170\text{--}180 \text{ km s}^{-1}$, which is higher than the typical velocity using the first kind of target.

The maximum velocity of the flow generated with the longest cylinder is $v_{\text{max}} \sim 180 \text{ km s}^{-1}$, which is slightly higher than the shortest one where $v_{\text{max}} \sim 170 \text{ km s}^{-1}$, even if the

mass which has to be put into motion is three times higher. This result is due to the interesting dynamics of transmitted and reflected shocks at each interface when the initial shock is launched (see figure 4). When the shock reaches the interface between the CH and the high-Z layer (see figure 4 (1)), the relative impedance of both layers leads to a transmitted shock which passes through the high-Z material and a reflected shock which goes back into the CH. The transmitted shock propagates through the high-Z layer, and when it reaches the layer of foam which has a lower impedance (see figure 4 (2)) a transmitted shock is produced in the foam and a rarefaction wave propagates back into the high-Z layer. Meanwhile, the reverse shock reaches the ablation front generated by the laser (see figure 4 (3)). There, a reflected shock appears and once again passes through the CH layer toward the high-Z layer and generates a second transmitted shock in the high-Z layer. This shock encounters the rarefaction wave (see figure 4 (4)) and accelerates until reaching the interface between the high-Z layer and the foam. There, it generates a second transmitted shock in the foam which goes faster than the first transmitted shock. Ultimately, if the foam layer is long enough, both shocks can coalesce (see figure 4 (5)). In this configuration the resulting shock is propagating faster into the foam and the asymptotic velocity of the expanding foam plasma is also higher. Considering the 1D numerical simulation presented in figure 3 of the target with the longest cylinder, the coalescence happens around 2 ns after the laser ignition once both shocks are approximately $100 \mu\text{m}$ away from the interface between the high-Z layer and the foam. That is why such an effect is not seen with the shorter cylinder: the first shock has already reached the bottom of the foam layer and the plasma has begun its expansion before the second shock can catch up with the first one.

Several leads are studied to produce a fast flow of plasma with a high enough velocity to get high post-shock temperature and to enhance radiative effects. In previous jet experiments a cone of foam has been used to generate a high Mach number flow. The properties of such jets are interesting in our context, so we investigate the behavior of a target with a conical mass reservoir instead of a cylindrical one. The complex propagation of transmitted and reflected shocks when the first launched shock is interacting with the cone wall helps in the collimation of the flow and should help to accelerate the material. The 1D approximation is no longer sustainable with this particular geometry. Then 2D simulations have been realized to investigate the behavior of the target (see figure 5). The cone angle had been optimized in the previous supersonic jet experiments and a parametric study validates the use of the same angle $\Phi = 77^\circ$ for our target configuration. The propagation of the initial shock into the cone leads to the formation of transmitted and reflected shocks when interacting with the cone wall, which can be seen at the early stage of the simulation (see figure 5, at $t = 5$ ns). The flow begins to expand into the tube after approximately $t_{\text{out}} = 7$ ns. While the flow expands, its interaction with the tube leads to the formation of shocks propagating inward in the middle of the tube (see figure 5, at $t = 17$ ns). At the late stage, when the flow hits the obstacle, the reverse shock is formed and begins to propagate upstream (see figure 5, at $t = 34$ ns). The typical velocity of the flow, with a foam initially with a density of 50 mg cm^{-3} , is around $u \sim 170 \text{ km s}^{-1}$ and the internal Mach number of the flow is approximately 10–20. The simulations are in agreement with the experimental regime published in Loupias *et al* (2007) (see table 1 in the present paper). The collision time is around $t = t_{\text{out}} + L_{\text{tube}}/u \sim 20$ ns, the typical post-shock density in the foam is of the order of 20 mg cm^{-3} , and the temperature is $T \propto u_{\text{flow}}^2 \sim 25 \text{ eV}$ (see figure 5). This temperature is lower than that obtained in the 1D simulations. This seems to be due to 2D effects: as an example, the loss of energy by the plasma while it interacts with the cone and the dissipation of part of the energy through transmitted shocks into the cone, which is not as efficient in the cylindrical

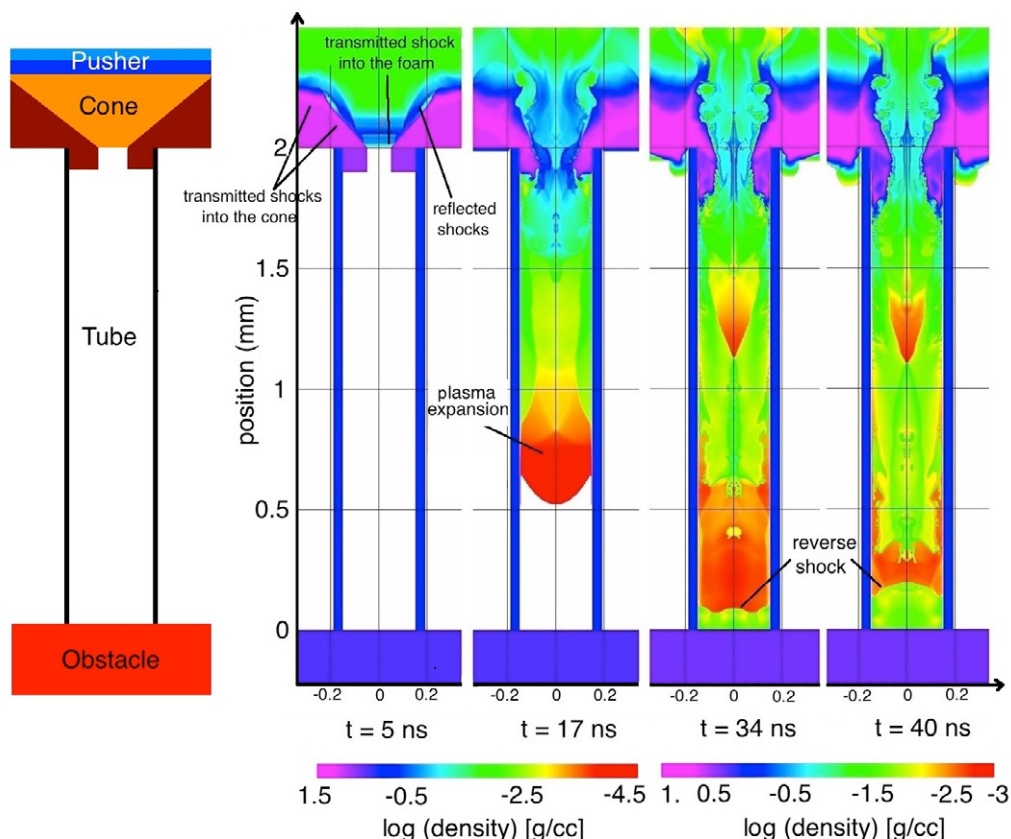


Figure 5. Evolution of the target with time; the color scale corresponds to the logarithm of density. At first the shock generated by the laser–matter interaction propagates through the cone of foam and reaches the bottom of the layer. The plasma expands into the tube which is filled with void. The flow hits the obstacle and a reverse shock is formed and propagates upstream. In this simulation, the tube is rigid. The initial density of the foam is 50 mg cm^{-3} .

case and which can be neglected as is done in the 1D simulations. The reverse shock propagates through the incoming material with a velocity of $u_{\text{rev.shock}} \sim 20 \text{ km s}^{-1}$ for $\sim 15 \text{ ns}$ and the Mach number characterizing this shock is of the order of 3.

4. Astrophysical relevance of laboratory experiments

The similarity properties concerning the two kinds of target and for the two different geometries of the mass reservoir are presented in table 2. To characterize the radiative regime in the post-shock flow, we give the order of magnitude for the Mach number of the reverse shock (M), the Boltzmann number (Bo) in the post-shock region which compares the enthalpy flux to the radiative energy flux, and finally, the cooling parameter (χ) also in the shocked region which represents the ratio of the characteristic cooling time to the dynamical one. Such characteristic numbers allow one to classify radiative shocks and highlight important physical processes at stake (Michaut *et al* 2009, Falize *et al* 2011a). In order to evaluate the thermodynamical quantities of the medium in the post-shock region, we look at the quantities profile when the

Table 2. Similarity properties of both kinds of target, from left to right: targets with a bi-layer plastic/titanium pusher; a target with a bi-layer of plastic/titanium and a cylinder of foam with l_1 length; a target with a bi-layer of plastic/titanium and a cylinder of foam with l_2 length; typical order of magnitude found in the astrophysical system. Orders of magnitude are taken inside the plastic for the first type of target and inside the foam for the second and third ones in 1D simulations, and inside the foam for the cone target in the 2D simulation done with the CEA code FCI2.

	CH/Ti	Cylinder mass equation	Cylinder length equation	Cone	Astrophysics system
v (km s ⁻¹)	130	170	180	170	5000
Post-shock density (g cm ⁻³)	0.15	0.03	0.04	0.02	5×10^{-8}
Post-shock temperature (eV)	45	35	45	25	10^4
M	2	4	2	3	> 10
Bo	10	5	4	10	...
χ	2	2	1	1	$\ll 1$

reverse shock is $\sim 100 \mu\text{m}$ away from the obstacle. At such a distance, the reverse shock can be diagnosed experimentally. The dynamical time is taken as equal to the ratio of the length of the shocked region divided by the sound velocity, representing the time needed for a perturbation to propagate across the shocked region. The cooling time is equal to the quotient of the internal energy density by the emissivity of the medium. This latter can be evaluated by multiplying σT^4 by the Planck mean opacity, where σ is the Stefan–Boltzmann constant.

At the astrophysical scale, we can estimate the order of magnitude for the velocity, density and temperature in the plasma by an analysis of spectroscopic and photometric data (see, e.g., Traulsen *et al* 2011). The Mach number which characterizes the reverse shock is of the order of 15–20, and the cooling parameter is very small compared to 1: radiative processes completely structure the post-shock region through their cooling effect.

Using a mass reservoir, we manage to create a supersonic flow of plasma with velocity of the order of 170–180 km s⁻¹, giving birth to a reverse shock characterized by Mach number of the order of 2–4, and which propagates for a period from a few nanoseconds to ~ 15 ns in a relatively homogeneous plasma of foam. This is an improvement compared to the first design, since we would like to get the fastest flow with the strongest possible reverse shock, and a homogeneous inflow similar to the astrophysical situation.

The new target design allows us to give more impact of the cooling on the post-shock structure. Indeed, the cooling parameter is smaller considering the use of a long mass reservoir. For the second kind of target, either considering the long cylinder or the cone, the post-shock flows are characterized by a χ parameter around 1. Consequently, radiative losses play a role in the dynamics, but do not strongly dominate the evolution of the plasma as in the astrophysical regime where $\chi \ll 1$. Then, even if better, this mixed regime is still not satisfactory for reproducing astrophysical flow. We would need a more efficient cooling system to obtain

similarity with the astrophysical flow. A higher speed of the flow would provide a higher post-shock temperature, which in turn could induce a more efficient radiative process to cool the flow more rapidly. Thus, we can assume that in higher-energy facilities, typical scales given in table 1 are accessible and still more relevant regimes for laboratory astrophysics can be reached.

The similarity properties obtained from the 2D simulations considering a mass reservoir with a conical geometry are more interesting than in the first target design using only a bi-layer pusher. We should note that one of the advantages of this kind of target is that the flow of foam generated into the tube is more diluted due to the propagation of the initial shock through all the cone length. Thus, the incoming foam medium into the tube is more homogeneous and its typical length is higher than with a cylindrical mass reservoir. This allows the reverse shock to propagate for a longer time into the plasma of foam, which is precisely the aim of the experiment. In the exhibited 2D numerical simulation, the reverse shock propagates for ~ 15 ns before passing through into the incoming titanium.

5. Conclusion

We have presented the experimental concept of the POLAR project similarity experiments. The latest improvements of the target are presented concerning, in particular, the mass reservoir. These new designs have been studied in order to get closer to similarity considering a kilojoule laser facility. Numerical simulations were performed to study the physics of the target, to define the best sizing compromise and to forecast regimes which can be reached in the laboratory. The additional mass reservoir makes it possible to produce a faster and more homogeneous flow. We also manage to get a reverse shock propagating for a longer time through the incoming flow by using a conical mass reservoir instead of a cylindrical one. Moreover, we showed that using a mass reservoir allows us to get a stronger reverse shock and also increases the influence of cooling processes on the post-shock structure, which is promising for similarity experiments in the context of polar accretion columns.

The first 1D simulations have to be complemented by 2D simulations to take into account the effects of the target geometry (cone, tube, etc). An experiment has been performed at the LULI2000 facility at the beginning of 2012 using the three target designs presented here. Experimental data are still in analysis and are to be compared to numerical simulations. Eventually, based on the results of this new experiment, work has to be done to pursue our effort to get closer to similarity with the astrophysical situation by improving the target design.

Acknowledgments

CB and CM acknowledge financial support from the 'Programme National de Physique Stellaire' (PNPS) of CNRS/INSU, France. CB, EF and CM also acknowledge financial support from the GdR PCHE in France and the Scientific Council of the Observatoire de Paris (France).

References

- Bluman G W and Cole J D 1974 *Similarity Methods for Differential Equations* (Berlin: Springer)
Busschaert C *et al* 2013 POLAR project: numerical modeling of the accretion column *High Energy Density Phys.* **9** 42

- Chevalier R A and Imamura J N 1982 Linear analysis of an oscillatory instability of radiative shock waves *Astrophys. J.* **261** 543–9
- Cropper M *et al* 1998 White dwarf masses in magnetic cataclysmic variables—multi-temperature FITS to GINGA data *Mon. Not. R. Astron. Soc.* **293** 222
- Falize É *et al* 2009 Scaling laws for radiating fluids: the pillar of laboratory astrophysics *Astrophys. Space Sci.* **322** 107–11
- Falize É *et al* 2011a Similarity properties and scaling laws of radiation hydrodynamic flows in laboratory astrophysics *Astrophys. J.* **730** 96
- Falize É, Dizière A and Loupiau B 2011b Invariance concepts and scalability of two-temperature astrophysical radiating fluids *Astrophys. Space Sci.* **336** 201–5
- Falize É *et al* 2011c The scalability of the accretion column in magnetic cataclysmic variables: the POLAR project *Astrophys. Space Sci.* **336** 81–5
- Falize É *et al* 2012 High-energy density laboratory astrophysics studies of accretion shocks in magnetic cataclysmic variables *High Energy Density Phys.* **8** 1–4
- Lamb D Q and Masters A R 1979 X and UV radiation from accreting magnetic degenerate dwarfs *Astrophys. J.* **234** L117–22
- Langer S H *et al* 1982 Time-dependent accretion onto magnetized white dwarfs *Astrophys. J.* **258** 289–305
- Larsson S 1992 Rapid optical variability in the AM Herculis object V834 Centauri. I—Quasi-periodic oscillations *Astron. Astrophys.* **265** 133–43
- Loupiau B *et al* 2007 Supersonic-jet experiments using a high-energy laser *Phys. Rev. Lett.* **99** 265001
- Michaut C *et al* 2009 Classification of and recent research involving radiative shocks *Astrophys. Space Sci.* **322** 77–84
- Norton A J *et al* 2008 The accretion flows and evolution of magnetic cataclysmic variables *Astrophys. J.* **672** 524–30
- Ramsay G and Cropper M 2004 The energy balance of polars revisited *Mon. Not. R. Astron. Soc.* **347** 497–507
- Ramsay G and Cropper M 2007 XMM-Newton observations of the eclipsing polar V2301 Oph *Mon. Not. R. Astron. Soc.* **379** 1209–16
- Remington B A *et al* 2006 Experimental astrophysics with high power lasers and Z pinches *Rev. Mod. Phys.* **78** 755–807
- Rybicki G B and Lightman A P 1986 *Radiative Processes in Astrophysics* (New York: Wiley-VCH)
- Ryutov D *et al* 1999 Similarity criteria for the laboratory simulation of supernova hydrodynamics *Astrophys. J.* **518** 821–32
- Savin D W *et al* 2012 The impact of recent advances in laboratory astrophysics on our understanding of the cosmos *Rep. Prog. Phys.* **75** 036901
- Schmidt G D *et al* 2005 New low accretion rate magnetic binary systems and their significance for the evolution of cataclysmic variables *Astrophys. J.* **630** 1037–53
- Schurtz G P, Nicolai PhD and Busquet M 2000 A nonlocal electron conduction model for multidimensional radiation hydrodynamics codes *Phys. Plasmas* **7** 4238–49
- Traulsen I *et al* 2011 XMM-Newton observations of the X-ray soft polar QS Telescopii *Astron. Astrophys.* **529** 116
- Warner B 1995 *Cataclysmic Variable Stars* (Cambridge: Cambridge University Press)
- Wickramasinghe D T and Ferrario L 2000 Magnetism in isolated and binary white dwarfs *Publ. Astron. Soc. Pac.* **112** 873–924
- Wu K *et al* 1994 Structure of steady state accretion shocks with several cooling functions: closed integral-form solution *Astrophys. J.* **426** 664–8
- Wu K 2000 Accretion onto magnetic white dwarfs *Space Sci. Rev.* **93** 611–49
- Zel'dovich Y B and Raizer Y P 1967 *Physics of Shock Waves and High-Temperature Hydrodynamic Phenomena* (New York: Academic)